

# The Baryon Census in a Multiphase Intergalactic Medium: One-Third of the Baryons are Still Missing

J. Michael Shull, Britton D. Smith<sup>1</sup>, & Charles W. Danforth

*CASA, Department of Astrophysical & Planetary Sciences,  
University of Colorado, Boulder, CO 80309*

michael.shull@colorado.edu, smit1685@msu.edu, charles.danforth@colorado.edu

## ABSTRACT

For low-redshift cosmology and galaxy formation rates, it is important to account for all the baryons synthesized in the Big Bang. Although galaxies and clusters contain  $\sim 10\%$  of the baryons, many more reside in the photoionized Ly $\alpha$  forest and shocked-heated warm-hot intergalactic medium (WHIM) at  $T \approx 10^{5-7}$  K. Current tracers of WHIM at  $10^{5-6}$  K include the O VI  $\lambda 1032, 1038$  absorption lines, together with broad Ly $\alpha$  absorbers (BLAs) and EUV/X-ray absorption lines from Ne VIII, O VII, and O VIII. We improve the O VI baryon surveys with corrections for oxygen metallicity ( $Z_{\text{O}}/Z_{\odot}$ ) and O VI ionization fraction ( $f_{\text{OVI}}$ ) using cosmological simulations of heating, cooling, and metal transport in a density-temperature structured medium. Statistically, their product correlates with column density,  $(Z_{\text{O}}/Z_{\odot}) f_{\text{OVI}} \approx (0.015)(N_{\text{OVI}}/10^{14} \text{ cm}^{-2})^{0.70}$ . The  $N_{\text{OVI}}$ -weighted mean is 0.01, which doubles previous estimates of WHIM baryon content. We also reanalyze H I data from the *Hubble Space Telescope*, applying redshift corrections for absorber density, photoionizing background, and proper length,  $dl/dz$ . We find substantial baryon fractions in the photoionized Ly $\alpha$  forest ( $28 \pm 11\%$ ), O VI/BLA-traced WHIM ( $25 \pm 8\%$ ), and collapsed phase ( $18 \pm 4\%$ ) in galaxies, groups, clusters, and circumgalactic gas. The baryon shortfall is  $29 \pm 13\%$ , which may be detected in X-ray absorbers from hotter WHIM or in weaker Ly $\alpha$  and O VI absorbers. Further progress will require higher-precision baryon surveys of weak absorbers at column densities  $N_{\text{HI}} \geq 10^{12.0} \text{ cm}^{-2}$ ,  $N_{\text{OVI}} \geq 10^{12.5} \text{ cm}^{-2}$ , and  $N_{\text{OVII}} \geq 10^{14.5} \text{ cm}^{-2}$ , with moderate-resolution UV and X-ray spectrographs.

*Subject headings:* cosmological parameters — observations — intergalactic medium — quasars: absorption lines

---

<sup>1</sup>now at Department of Physics and Astronomy, Michigan State University, East Lansing, MI 48824

## 1. INTRODUCTION

Cosmologists have noted a baryon deficit in the low-redshift universe (Fukugita, Hogan, & Peebles 1998) relative to the predicted density synthesized in the Big Bang. Although this deficit may arise from an incomplete inventory, it could also challenge our understanding of the thermodynamics of structure formation and the response of the intergalactic medium (IGM) to accretion shocks and galactic outflows. Recent analysis (Komatsu et al. 2011) of the spectrum of acoustic peaks in the Cosmic Microwave Background (CMB) obtained by the *Wilkinson Microwave Anisotropy Probe* (WMAP) found that baryons comprise a fraction  $\Omega_b = 0.0455 \pm 0.0028$  of the critical matter-energy density,  $\rho_{\text{cr}} = (9.205 \times 10^{-30} \text{ g cm}^{-3})h_{70}^2$ , of the universe, where  $h_{70}$  is the Hubble constant ( $H_0$ ) in units of  $70 \text{ km s}^{-1} \text{ Mpc}^{-1}$ . This 4.6% baryon fraction corresponds to a comoving density,  $\rho_b = \Omega_b \rho_{\text{cr}} = 4.24 \times 10^{-31} \text{ g cm}^{-3}$ , and a hydrogen number density  $n_H = 1.90 \times 10^{-7} \text{ cm}^{-3}$ , assuming a primordial helium mass fraction  $Y_p = 0.2477$  (Peimbert et al. 2007).

Galaxy surveys find  $\sim 10\%$  of these baryons in collapsed objects such as galaxies, groups, and clusters (Salucci & Persic 1999; Bristow & Phillipps 1994; Fukugita & Peebles 2004). Another 5% may reside in condensed gas in the circumgalactic medium (CGM) within the virial radius of galaxies. Of the remaining 85–90%, only half has been accounted for in the low- $z$  IGM (Shull 2003; Bregman 2007; Danforth & Shull 2008; Danforth 2009). The remainder appears to be gravitationally unbound gas, distributed between the galaxies in the IGM or CGM. An inefficient distribution of collapsed baryons vs. distributed matter is a prediction of nearly all cosmological simulations of large-scale structure formation (Cen & Ostriker 1999, 2006; Davé et al. 1999, 2001; Smith et al. 2011). These N-body hydrodynamical simulations suggest that 10–20% of the baryons reside in collapsed objects and dense filaments, with the remaining 80% in the IGM or CGM. At low redshifts, intergalactic matter exists over a wide range of phases in baryon overdensity ( $\Delta_b = \rho_b/\bar{\rho}_b$ ) and temperature ( $T$ ). Cosmological simulations suggest that  $\sim 30\%$  resides in diffuse photoionized IGM filaments, observable as the low- $z$  “Lyman- $\alpha$  forest” of absorption lines (Penton et al. 2000, 2004; Lehner et al. 2007). Another 30–40% is contained in the shock-heated IGM at  $10^5 \text{ K}$  to  $10^7 \text{ K}$ , a phase often termed the warm-hot intergalactic medium (WHIM).

Thermodynamic considerations suggest that a substantial amount of shock-heated IGM at  $z < 1$  is an expected consequence of gravitational instability in a dark-matter dominated universe. Additional hot gas is produced by galactic-wind shocks and virialization in galaxy halos. Owing to its low density, the “Cosmic Web” of intergalactic filaments is difficult to detect in emission. More promising are absorption-line studies, which use the high ionization states of abundant heavy elements, whose resonance lines fall in the far-ultraviolet (C IV, N V, O VI), extreme ultraviolet (O IV, O V, Ne VIII), and soft X-ray (O VII, O VIII, N VI,

Ne IX). The low- $z$  WHIM has most effectively been surveyed in the O VI resonance lines at 1031.926 Å and 1037.617 Å (Danforth & Shull 2005, 2008; Tripp et al. 2008; Thom & Chen 2008), which probe the temperature range  $10^{5.3-5.7}$  K in collisionally ionized gas. A few detections of weak Ne VIII have also been reported (Savage et al. 2005; Narayanan et al. 2009, 2011) probing somewhat hotter gas. These weak X-ray absorption lines are difficult to detect with the current throughput and spectral resolution of spectrographs on *Chandra* and *XMM/Newton*. Possible X-ray detections of hotter gas at  $(1 - 3) \times 10^6$  K have been claimed, using weak absorption lines of helium-like O VII  $\lambda 21.602$  (Nicastro et al. 2005a,b, 2008; Buote et al. 2009; Fang et al. 2010; Zappacosta et al. 2010) and hydrogenic O VIII  $\lambda 18.969$  (Fang et al. 2002, 2007). Most of these *Chandra* detections remain controversial, because they are unconfirmed by the *XMM-Newton* satellite (Kaastra et al. 2006; Williams et al. 2006; Rasmussen et al. 2007). Recent analyses of spectroscopic data on Mrk 421 fails to detect any WHIM gas at the claimed redshifts ( $z = 0.01$  and  $0.027$ ), either in broad Ly $\alpha$  absorption (Danforth et al. 2011) from high-S/N data from the Cosmic Origins Spectrograph (COS) on the *Hubble Space Telescope (HST)* or in O VII (Yao et al. 2012) in *Chandra* data.

Thus, the baryon census at low redshift remains uncertain. Although UV surveys of intergalactic Ly $\alpha$  and O VI absorbers have accumulated substantial numbers, the claimed X-ray WHIM detections (O VII, O VIII) do not yet provide reliable measures of the baryon reservoir at  $T > 10^6$  K. In this paper, we examine the baryon content in various IGM phases, with the aim of determining the accuracy of the observational and numerical estimates. In particular, the Ly $\alpha$  absorption surveys probe the small neutral component of diffuse (photoionized) filaments and require correction for the neutral ionization fraction ( $f_{\text{HI}}$ ). The O VI surveys must be corrected for O VI ionization fraction and oxygen metallicity in order to derive their contribution to the WHIM. Danforth & Shull (2008) measured the column densities of 83 O VI absorbers and estimated that  $8.6 \pm 0.8\%$  of the baryons reside in this phase, using constant correction factors for the oxygen metallicity ( $Z_{\text{O}} \approx 0.1 Z_{\odot}$ ) and O VI ionization fraction ( $f_{\text{OVI}} = 0.2$ ).

To constrain the range of  $Z_{\text{O}}$  and  $f_{\text{OVI}}$ , we use simulations of IGM heating, cooling, and metal transport to find the column-density weighted average for their product,  $(Z_{\text{O}}/Z_{\odot}) f_{\text{OVI}}$ . Our computed value, 0.01 or half the previously assumed value, doubles the previous estimate of the baryon census traced by O VI. In Section 2 we describe the simulations and their results for the O VI distribution in column density, gas temperature, baryon overdensity, metallicity, and ionization fraction. In Section 3, we assess the corrections for ionization and metallicity, applied to the O VI and Ly $\alpha$  absorbers and derive values of  $\Omega_b$  from recent surveys of each IGM phase. Variations in these factors are produced by WHIM thermodynamics, gas temperature ( $T$ ), baryon overdensity ( $\Delta_b$ ), and O VI column density ( $N_{\text{OVI}}$ ). In Section 4, we summarize the current baryon census with uncertainties.

## 2. COSMOLOGICAL SIMULATIONS OF THE WHIM

The simulation analyzed in this work is run 50\_1024.2 of Smith et al. (2011), performed with the adaptive-mesh-refinement + N-body code **Enzo** (Bryan & Norman 1997; O’Shea et al. 2004). Post-processing of the simulations was performed using the data analysis and visualization package, **yt**<sup>1</sup>, documented by Turk et al. (2011). The simulation has a box size of  $50h^{-1}$  Mpc comoving, with  $1024^3$  grid cells and dark matter particles, giving it a dark-matter mass resolution of  $7 \times 10^6 M_\odot$  and spatial cells of  $50h^{-1}$  kpc. Radiative cooling is included by solving for the non-equilibrium chemistry and cooling of atomic H and He, coupled to tabulated metal cooling rates computed as a function of density, metallicity, temperature, electron fraction, and redshift, in the presence of an ionizing metagalactic radiation background. To mimic the effects of reionization, we include a spatially uniform, but redshift-dependent radiation background given by Haardt & Madau (2001). The influence of the radiation background through photoheating and photoionization is included in the cooling of both the primordial and metal species.

We employ a modified version of the star-formation routine of Cen & Ostriker (1992). Star particles, representing the combined presence of a few million solar masses of stars, are formed when the following three conditions are met: the total density of a grid cell is above a certain threshold, a convergent flow exists (negative velocity divergence), and the cooling time is less than the dynamical time. Star particles return feedback to the grid in the form of metal-enriched gas and thermal energy. We use a distributed-feedback method (Smith et al. 2011) in which material and energy are distributed over a 27-cell cube (three cells on a side) centered on the location of the star particle. This is done to mitigate the over-cooling that occurs when feedback is deposited into a single grid cell, which raises the temperature, gas density, and cooling rate to unphysically high values. Over-cooling also causes the winds that should be transporting metals into the IGM to fizzle out and remain confined to their sites of origin. Smith et al. (2011) showed that this model is able simultaneously to provide good matches to the global star formation history and the observed number density per unit redshift of O VI absorbers (Danforth & Shull 2008). If all three above conditions are satisfied, then a “star particle,” representing a large collection of stars, is formed within the grid cell with a total mass,  $m_* = f_* m_{\text{cell}} (\Delta t / t_{\text{dyn}})$ . Here,  $f_* \approx 0.1$  is the star-formation efficiency,  $m_{\text{cell}}$  is the baryon mass in the cell,  $t_{\text{dyn}}$  is the dynamical time, and  $\Delta t$  is the hydrodynamical timestep. Subsequently, this much mass is also removed from the grid cell as the star particle is formed, ensuring mass conservation. Although the star particle is formed instantaneously within the simulation, feedback is assumed to occur over a longer time scale, which more

---

<sup>1</sup><http://yt.enzotools.org/>

accurately reflects the gradual process of star formation. Stellar feedback is represented by the injection of thermal energy and the return of gas and metals to the grid, in amounts proportional to  $\Delta m_{\text{sf}}$ . We assume that a fraction (25%) of the stellar mass is returned to the grid as gas. The thermal energy and metals returned to the grid are  $e = \epsilon(\Delta m_{\text{sf}})c^2$  and  $m_{\text{metals}} = (\Delta m_{\text{sf}})y$ , where  $\epsilon \approx 10^{-5}$  is the ratio of rest-mass energy to thermal energy and  $y \approx 0.025$  is the metal yield. The rate of star formation, and hence the rate at which thermal energy and metals are injected into the grid by the star particle, peaks after one dynamical time, then decays exponentially.

In the current project, we seek to understand the thermal and ionization state of the IGM, including the covariance of metallicity, temperature, and O VI ionization fraction. In our simulations, the physical properties of O VI absorbers and the degree to which they trace the WHIM are in good agreement with other recent simulations (Tepper-Garcia et al. 2011; Cen & Chisari 2011). However, they differ significantly from those of Oppenheimer & Dave (2009, 2011), who found that O VI and Ne VIII originate almost exclusively in warm ( $T \approx 10^4$  K), photoionized gas. Tepper-Garcia et al. (2011) suggested that much of this difference arises because Oppenheimer & Davé (2009) neglected the effect of photoionization on metal-line cooling. Oppenheimer et al. (2011) investigated this claim by running additional simulations in which photoionization reduced the metal cooling. This reduction resulted in a small, but insufficient number of O VI absorbers associated with WHIM gas. Instead, they point to the fact that they do not include the mixing of metals from their galactic-wind particles, allowing feedback to take on the form of cold, heavily enriched clouds.

In examining the various interpretations of the high ions (O VI and Ne VIII), we have identified several key differences between the two codes: the Oppenheimer-Davé smooth particle hydrodynamic (SPH) code and our grid-based approach with **Enzo**. The disagreement between the IGM temperatures and ionization mechanisms appear to arise from four effects: (1) Different methods of injecting energy and metals (mixed or unmixed); (2) Over-cooling of unmixed, metal-enriched gas at high density and high metallicity; (3) Differences in shock capturing (and shock-heating) between SPH and grid codes; (4) Differences in photoionization rates through the assumed radiation fields at  $h\nu = 100 - 250$  eV. All four possibilities merit careful comparative studies. The resolution of this O VI controversy may ultimately hinge on understanding the nature of galactic winds and their ability to mix heavy elements into the IGM.

### 3. CENSUS OF BARYONS IN DIFFERENT THERMAL PHASES

The results of our simulations relevant to O VI are illustrated in Figures 1–6. Figure 1 shows the temperature-density phase diagram of the multiphase IGM, color-coded by baryon mass fraction. The commonly found features include the diffuse Ly $\alpha$  absorbers (temperatures  $T = 10^{3.0-4.5}$  K and baryon overdensities  $\Delta_b = 10^{-2}$  to  $10^{+1.5}$ ), a condensed phase ( $\Delta_b > 10^3$ ), and a shocked-heated plume of WHIM gas ( $T = 10^{5-7}$  K and  $\Delta_b = 10^0$  to  $10^{2.5}$ ). The gas traced by O VI typically resides at temperatures  $5 < \log T < 6$ . Figure 2 shows the simulated cumulative mass distribution of O VI versus column density. Evidently, a significant fraction of O VI is traced by weak absorbers with  $\log N_{\text{OVI}} \leq 13.5$ .

Our simulations show a large variation (and covariance) of the O VI properties, including metallicity, temperature, and ionization fraction. Figures 3 and 4 show the range and covariance of the two correction factors: oxygen metallicity in solar units ( $Z_{\text{O}}/Z_{\odot}$ ) and O VI ionization fraction  $f_{\text{OVI}}$ . The ionization fraction includes the effects of both collisional ionization and photoionization, as discussed in detail by Smith et al. (2011). Figure 3 color-codes these distributions in  $N_{\text{OVI}}$ , while Figure 4 illustrates their distribution in temperature and baryon overdensity. The wide range of physical conditions in which O VI exists demonstrates the multiphase character of this ionized gas. The mechanisms that produce the O VI (113.87 eV) include collisional ionization (CI) at  $\log T > 5$  and photoionization (PI) by the hard (EUV) metagalactic background. The dashed line in Figure 4 shows the locus of points ( $\log T$  and  $\log \Delta_b$ ) at which  $\text{CI} = \text{PI}$ . This calculation is based on O V collisional ionization rates from Shull & Van Steenberg (1982). The O V photoionization rate was derived, assuming a cross section  $\sigma(E) = (0.36 \times 10^{-18} \text{ cm}^2)(E/113.87 \text{ eV})^{-2.1}$  and the EUV radiation field at 8–10 ryd from Figure 13 of Haardt & Madau (2011).

Figure 5 shows the distribution of the product,  $(Z_{\text{O}}/Z_{\odot}) f_{\text{OVI}}$ , throughout the simulation. Color-coded by O VI mass fraction, this plot shows bimodality of this product with temperature and baryon overdensity. In the deepest-red portions, representing high O VI mass fraction, one finds regions with large values,  $(Z_{\text{O}}/Z_{\odot}) f_{\text{OVI}} \approx 10^{-1.3}$ , in the high-density filaments with  $\Delta_b \approx 100$ , and other regions with lower values,  $(Z_{\text{O}}/Z_{\odot}) f_{\text{OVI}} \approx 10^{-2.5}$  at  $\Delta_b \approx 10$ . In converting the column densities of O VI absorbers to baryons, one should not adopt single corrections for metallicity and ionization fraction. However, as we discuss in Section 3.1, one can apply statistical corrections that correlate the product  $(Z_{\text{O}}/Z_{\odot}) f_{\text{OVI}}$  with O VI column density (Figure 6). Integrating over the O VI column-density distribution, we find that this product is a factor of two lower than the previously assumed value of 0.02. This doubles the fraction of WHIM baryons traced by O VI from 7-8% to  $15 \pm 4\%$ .

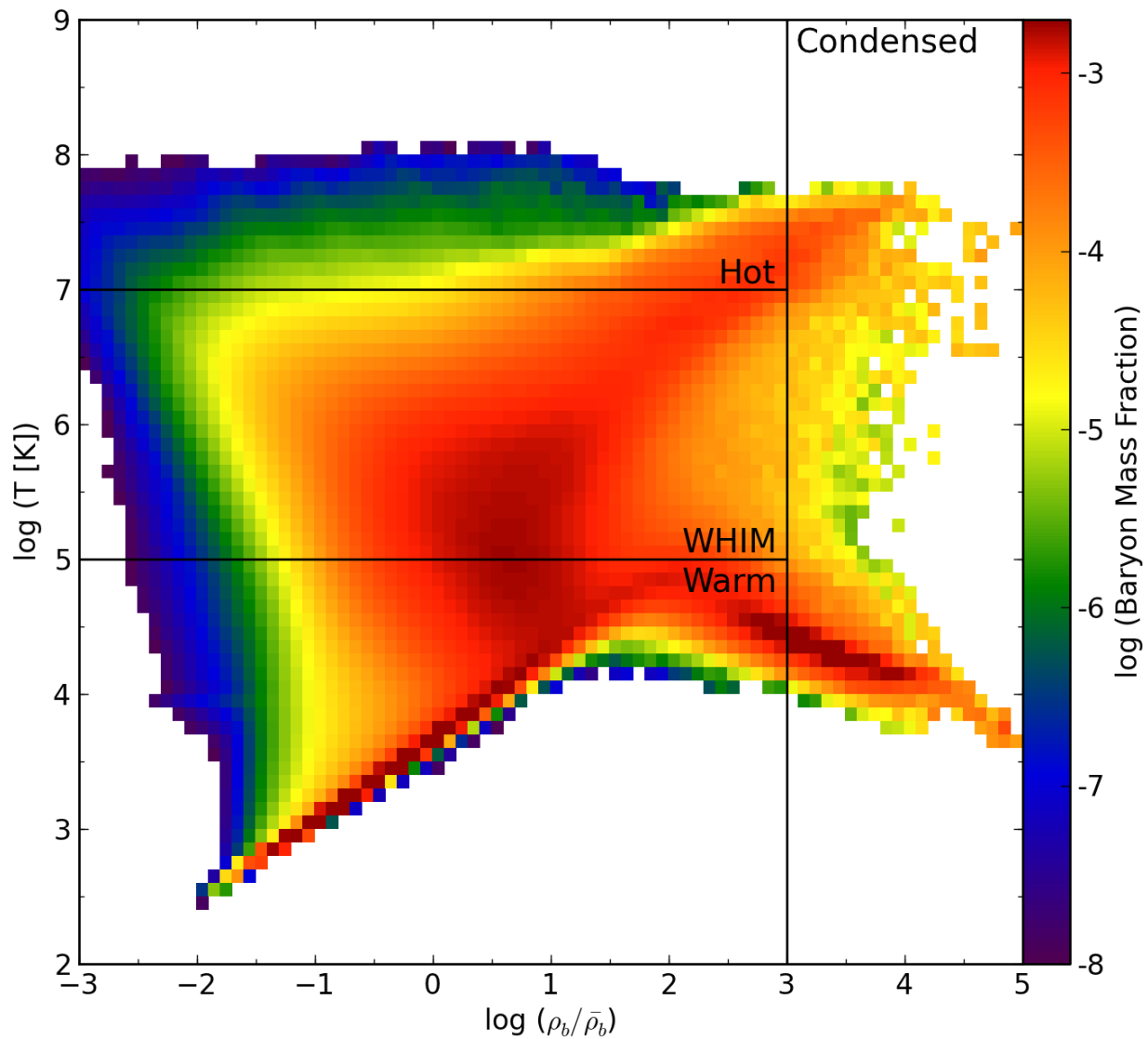


Fig. 1.— Distribution of IGM in temperature  $T$  and baryon overdensity  $\Delta_b = \rho_b/\bar{\rho}_b$ , color-coded by baryon mass fraction. This distribution shows the same thermal phases seen in simulations by other groups and commonly labeled as warm (diffuse photoionized gas), WHIM, and condensed.

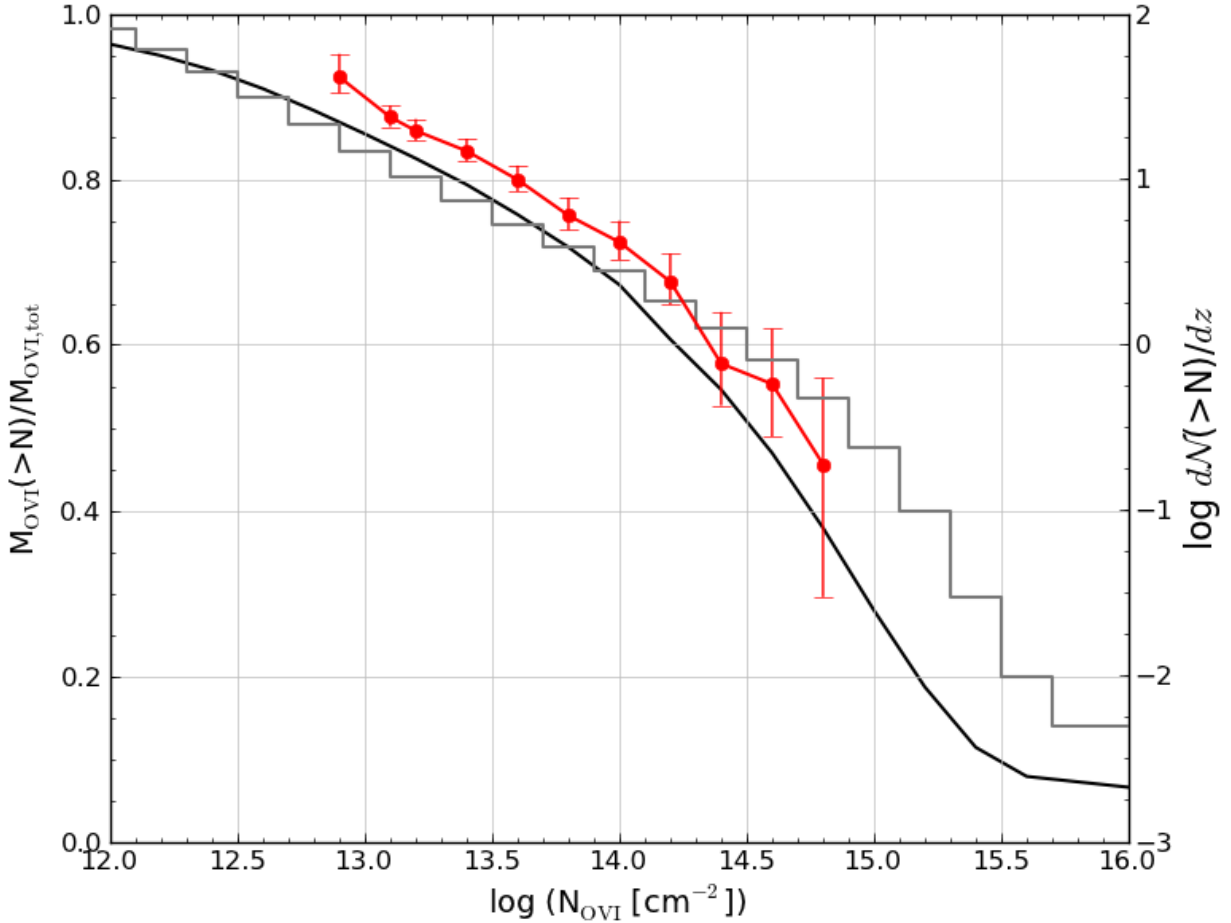


Fig. 2.— Cumulative distribution of O VI by mass from our WHIM simulation, for column densities  $N_{\text{OVI}} = 10^{12}$  to  $10^{16} \text{ cm}^{-2}$ . Solid black line shows cumulative mass fraction, labeled on left vertical axis. Gray histogram shows cumulative number of O VI absorbers, labeled on right vertical axis. Red points show observed cumulative column-density distribution (Danforth & Shull 2008) labeled on right vertical scale. A significant fraction of O VI-traced WHIM resides in weak absorbers, although the distribution flattens at  $\log N_{\text{OVI}} \leq 13.5$ .



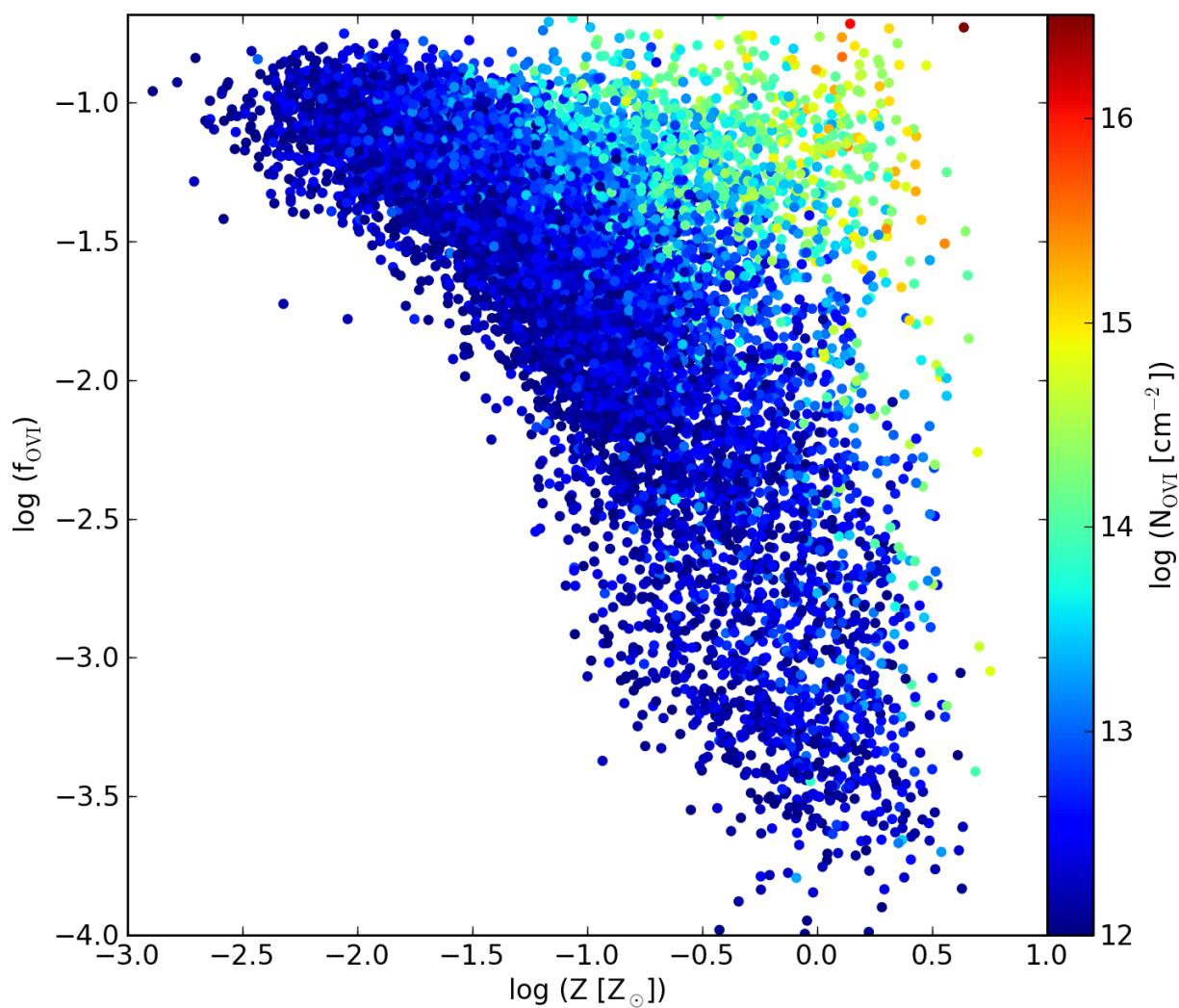


Fig. 3.— Distribution of IGM metallicity ( $Z/Z_{\odot}$ ) and O VI ionization fraction ( $f_{\text{OVI}}$ ) color-coded by O VI column density. Note the wide range and covariance of individual factors, whose product,  $f_{\text{OVI}}(Z/Z_{\odot})$ , correlates with O VI column density (color bar along right).

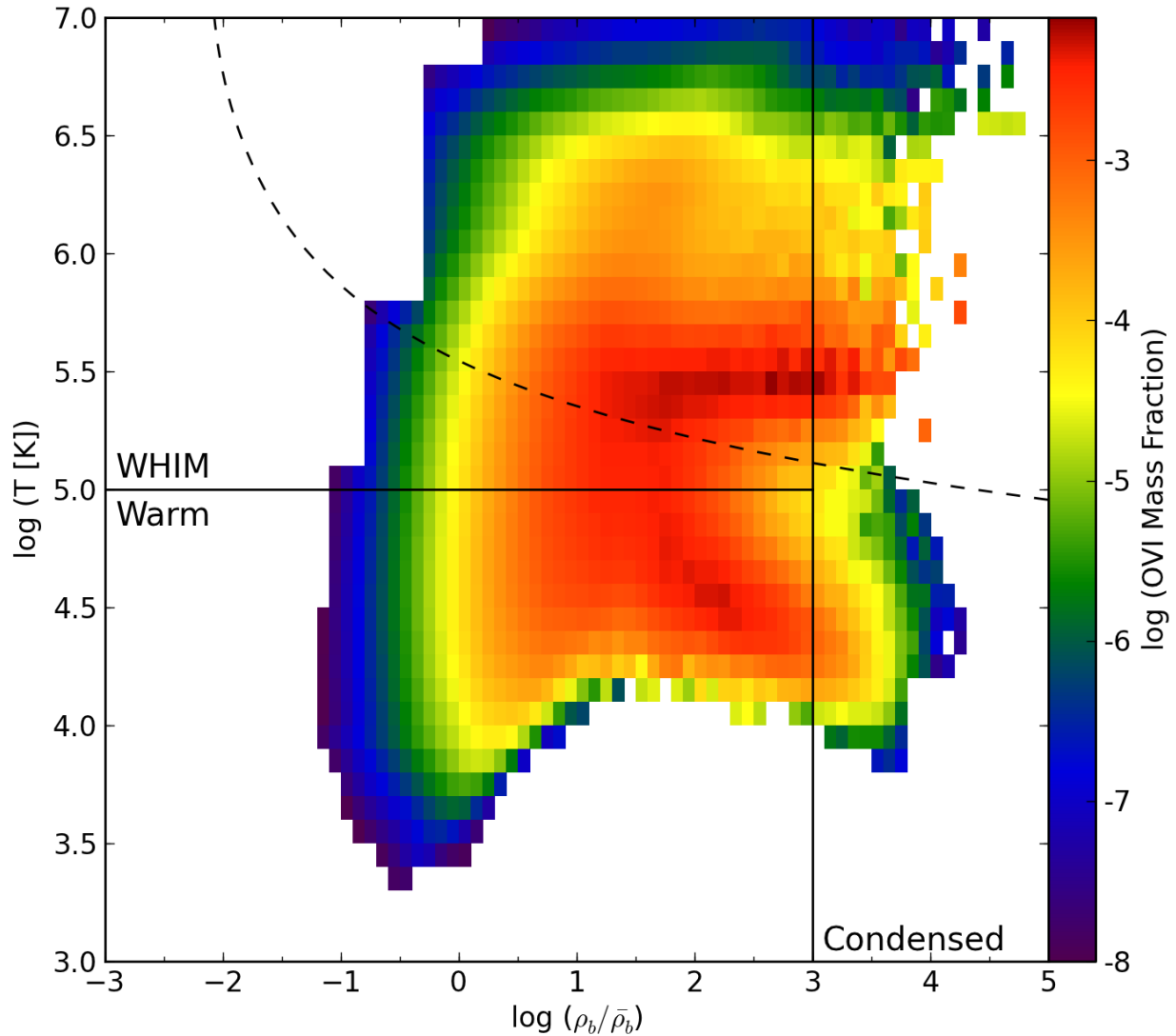


Fig. 4.— Distribution of IGM temperature versus baryon overdensity,  $\Delta_b = \rho_b/\bar{\rho}_b$ , color-coded by O VI mass fraction. In this phase space, we identify the WHIM ( $T \geq 10^5$  K), warm, diffuse photoionized gas ( $T < 10^5$  K and  $\Delta_b < 1000$ ), and condensed gas ( $\Delta_b > 1000$ ). Dashed line shows locus at which collisional ionization equals photoionization (collisional ionization dominates above the dashed curve).

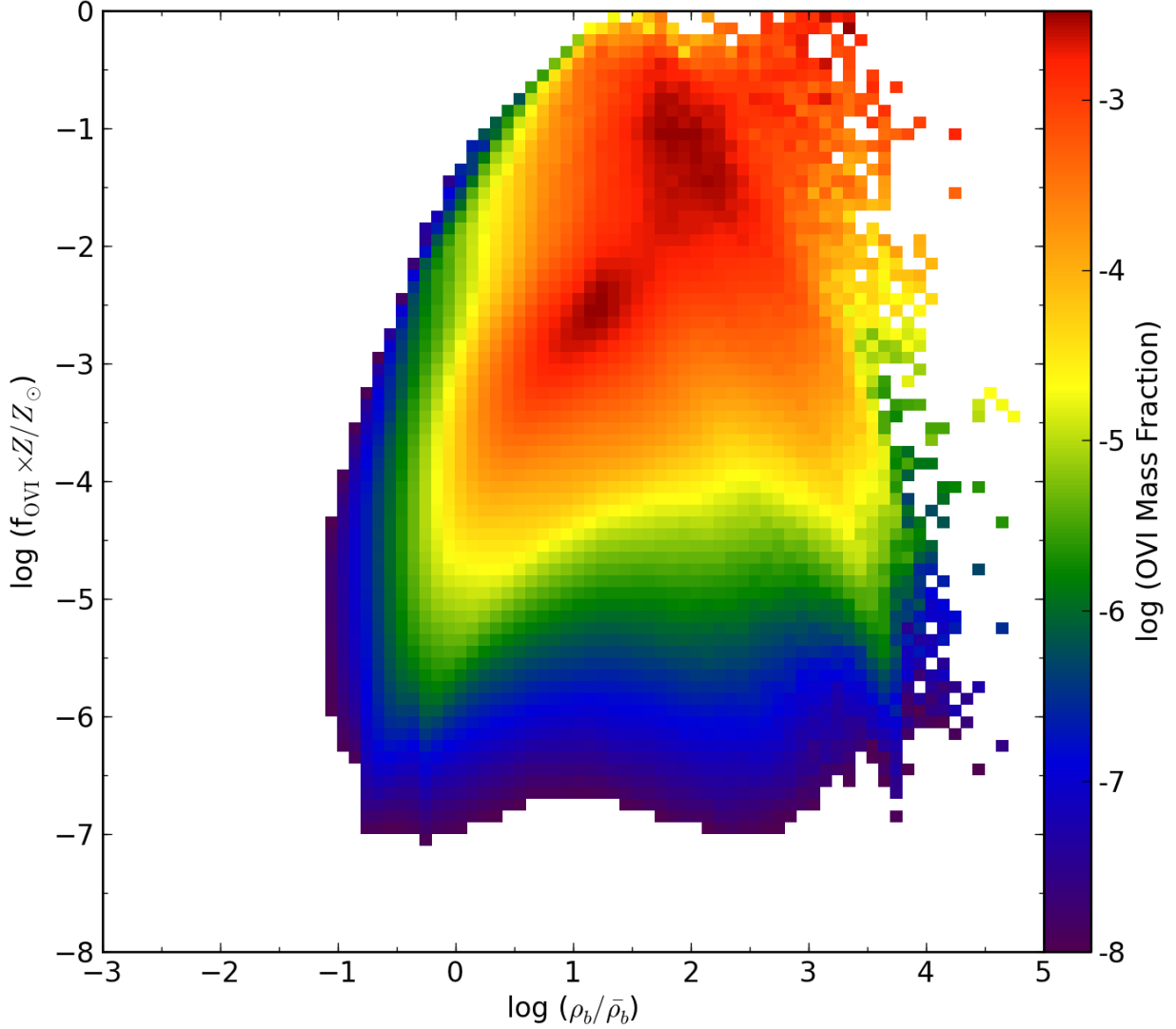


Fig. 5.— Distribution of the metallicity-ionization product,  $(Z_{\text{O}}/Z_{\odot}) f_{\text{OVI}}$ , versus baryon overdensity,  $\Delta_b = \rho_b/\bar{\rho}_b$ , color-coded by O VI mass fraction. The broad distribution of the product, from 0.001 to 0.1 has local enhancements (deep red) in low-metallicity regions (overdensities  $\Delta_b \approx 10$ ) and high-metallicity regions ( $\Delta_b \approx 100$ ). The column density weighted mean of this product is 0.01 (see Fig. 6).

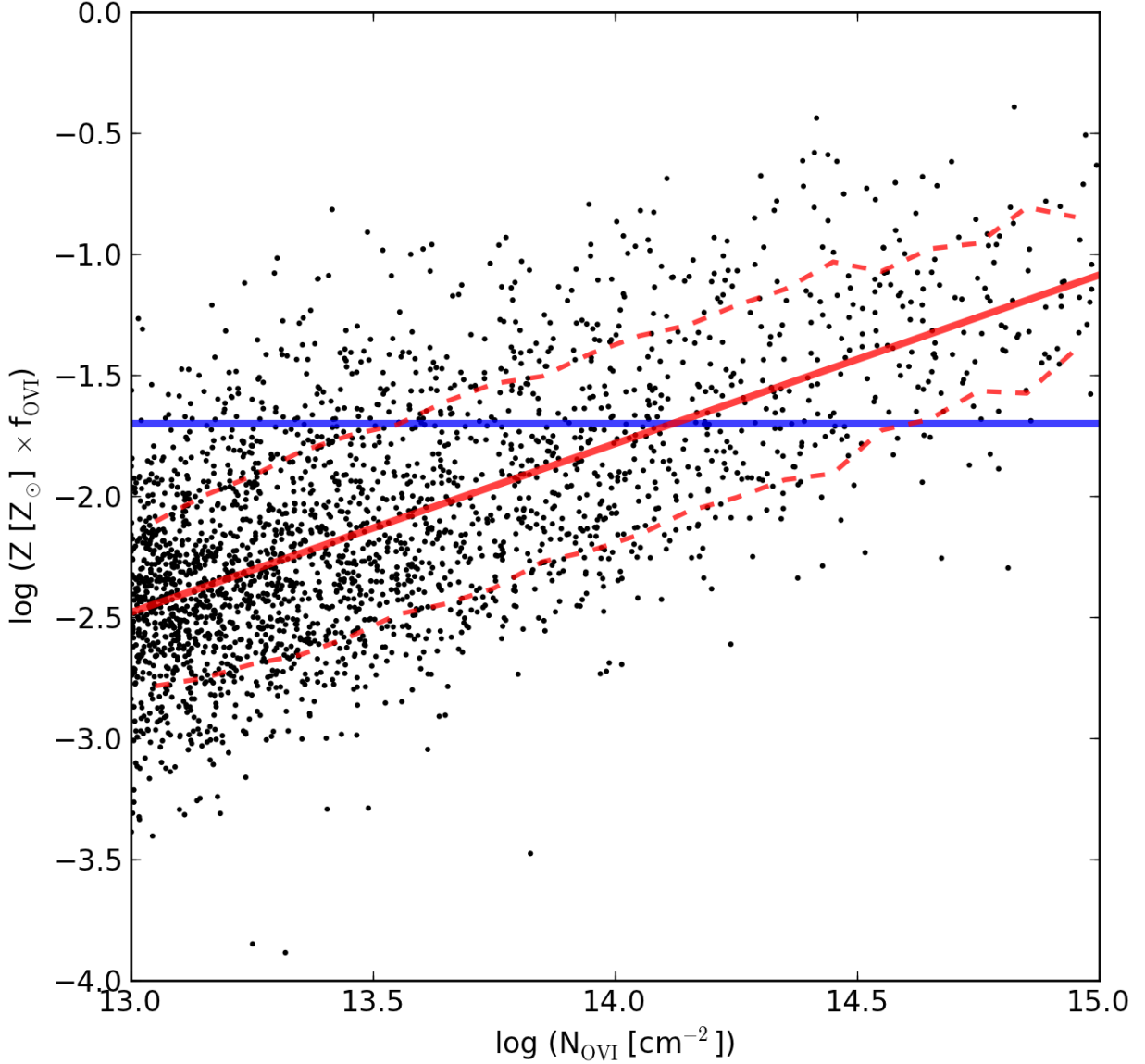


Fig. 6.— Values of the product,  $(Z_{\text{O}}/Z_{\odot}) f_{\text{OVI}}$ , for the WHIM simulation, overlaid with a power-law fit (solid red line) to the ensemble,  $(0.015)[N_{\text{OVI}}/10^{14} \text{ cm}^{-2}]^{0.70}$ . Integrating over the observed distribution in  $N_{\text{OVI}}$ , we find a weighted value of 0.01. Horizontal (blue) line shows previously assumed value of 0.02 for this product ( $Z/Z_{\odot} = 0.1$  and  $f_{\text{OVI}} = 0.2$ ). Typical variance ( $1\sigma$ ) about this fit is 0.3-0.4 dex, shown by red dashed lines.

### 3.1. Warm-Hot IGM Probed in O VI Absorption

As noted, the metallicity and O VI ionization fraction vary throughout the grid in the simulated IGM. Figures 5 and 6 show that the *product* of  $f_{\text{OVI}}$  and  $Z_{\text{O}}$  correlates with  $N_{\text{OVI}}$ , with weaker absorbers having systematically lower values. This is primarily an effect of spatial variations in the metallicity, but also variations in the ionization fraction,  $f_{\text{OVI}}$ , produced by spatial fluctuations in WHIM temperature and contributions from photoionizing radiation on low-density IGM. The baryon content in O VI-traced WHIM is given by an integral over O VI column density ( $N$ ), now with the corrections for metallicity and ionization fraction placed inside the integral:

$$\Omega_b^{(\text{OVI})} = \left[ \frac{\mu_b H_0}{c \rho_{\text{cr}} (\text{O}/\text{H})_{\odot}} \right] \int_{N_{\text{min}}}^{N_{\text{max}}} \frac{d\mathcal{N}(N)}{dz} \frac{N}{Z_{\text{O}}(N) f_{\text{OVI}}(N)} dN . \quad (1)$$

Here,  $\mu_b = 1.33m_H$  is the mean baryon mass per hydrogen nucleus, accounting for helium. Earlier surveys that used O VI as a baryon tracer assumed constant values of the O VI ionization fraction,  $f_{\text{OVI}} = 0.2$  (its maximum value in collisional ionization equilibrium at  $\log T_{\text{max}} = 5.45$ ) and metallicity,  $Z_{\text{O}}/Z_{\odot} = 0.1$ , relative to the solar oxygen abundance,  $(\text{O}/\text{H})_{\odot} = 4.90 \times 10^{-4}$  (Asplund et al. 2009).

From our simulations, we analyze the variation of metallicity and ionization to produce a statistical correlation (Figure 6) between the product of oxygen metallicity and O VI ionization fraction. We find a power-law dependence on O VI column density, scaling as  $N^{\gamma}$ ,

$$(Z_{\text{O}}/Z_{\odot}) f_{\text{OVI}} = (0.015)(N_{\text{OVI}}/10^{14} \text{ cm}^{-2})^{0.70} . \quad (2)$$

Integrated over the observed distribution  $d\mathcal{N}/dz \propto N^{-\beta}$ , we find

$$\Omega_b^{(\text{OVI})} \propto \int_{N_{\text{min}}}^{N_{\text{max}}} N^{1-\gamma-\beta} dN \propto [N_{\text{min}}^{2-\gamma-\beta} - N_{\text{max}}^{2-\gamma-\beta}] . \quad (3)$$

For our fitted  $\gamma \approx 0.70$  and the observed  $\beta \approx 2.0$  (Danforth & Shull 2008), the integral increases at the low end as  $N_{\text{min}}^{-0.7}$ . The column-density weighted mean of the product  $f_{\text{OVI}}(Z_{\text{O}}/Z_{\odot}) = 0.01$ , a factor of two smaller than previously assumed. For our standard integration range,  $13.0 \leq \log N_{\text{OVI}} \leq 15.0$ , this correction doubles the number of baryons in the O VI-traced WHIM, compared to previous assumptions.

There have been a number of previous O VI surveys and baryon estimates, quantified by an absorption-line frequency,  $d\mathcal{N}/dz$ , per units redshift and an O VI-traced baryon fraction,  $\Omega_b^{(\text{OVI})}/\Omega_b$ . Using 40 O VI absorbers seen with *FUSE*, Danforth & Shull (2005) found  $d\mathcal{N}/dz \approx 17 \pm 3$  for column densities  $13.0 \leq N_{\text{OVI}} \leq 14.5$ . The  $10^{13} \text{ cm}^{-2}$  lower limit

corresponds to 30 mÅ equivalent width in O VI  $\lambda$ 1032. The 2005 census gave an O VI-traced baryon fraction of at least  $4.8 \pm 0.9\%$  (statistical error only) for a correction factor  $f_{\text{OVI}}(Z_{\text{O}}/Z_{\odot}) = 0.02$ . Danforth & Shull (2008) used *HST*/STIS data on 83 O VI absorbers to find  $d\mathcal{N}/dz \approx 15.0^{+2.7}_{-2.0}$  integrated to 30 mÅ, and  $d\mathcal{N}/dz \approx 40^{+14}_{-8}$  to 10 mÅ. The derived WHIM baryon fractions in this 2008 census were  $7.3 \pm 0.8\%$  and  $8.6 \pm 0.8\%$ , integrated to 30 mÅ and 10 mÅ, respectively. For comparison, Tripp et al. (2008) found a similar line frequency,  $d\mathcal{N}/dz \approx 15.6^{+2.0}_{-2.4}$  for 51 intervening O VI absorption systems integrated to 30 mÅ, while Thom & Chen (2008) found  $d\mathcal{N}/dz \approx 10.4 \pm 2.2$  for 27 O VI absorbers down to 30 mÅ. However, the latter survey required detection of both O VI lines at 1032 Å and 1038 Å, and should be regarded as a lower limit.

As part of a Hubble Archive Legacy project (PI: Shull, HST-AR-11773.01), the Colorado group has reanalyzed the *HST*/STIS data on IGM absorption lines. In a future publication (E. Tilton et al. 2012, in preparation), we will provide details of our new survey, which finds 111 O VI absorbers and corrects for a few identification errors in Danforth & Shull (2008). They establish more reliable baryon fractions for the O VI-traced WHIM of  $6.2 \pm 0.6\%$  (to 30 mÅ) and  $7.6 \pm 0.5\%$  (to 10 mÅ), using the old correction-factor product,  $f_{\text{OVI}}(Z_{\text{O}}/Z_{\odot}) = 0.02$ . Taken as a whole, these O VI surveys suggest a typical WHIM baryon fraction of approximately 7.5%, assuming the old values,  $(Z_{\text{O}}/Z_{\odot}) = 0.1$  and  $f_{\text{OVI}} = 0.2$ . If we adopt our new correction factors,  $f_{\text{OVI}}(Z_{\text{O}}/Z_{\odot}) = 0.01$ , the baryon fractions double. In this paper, we adopt an O VI-traced baryon fraction of  $15 \pm 4\%$ , where we have increased the error to account for systematic uncertainties. The value of  $\Omega_b^{(\text{OVI})}$  is dominated by weaker absorbers with  $N_{\text{OVI}} < 10^{13.5} \text{ cm}^{-2}$ , where the absorption-line statistics become uncertain. An accurate O VI census will require measuring weaker O VI  $\lambda$ 1032 absorption lines, with column densities below  $10^{13} \text{ cm}^{-2}$ , corresponding to equivalent widths  $W_{\lambda} = (12.5 \text{ mÅ})(N_{\text{OVI}}/10^{13} \text{ cm}^{-2})$ . Deep spectroscopic surveys in O VI can also ascertain where the distribution of O VI absorbers flattens (see Fig. 2).

### 3.2. Diffuse Photoionized Ly $\alpha$ Filaments

As described in Penton et al. (2000), the photoionization correction for the H I (Ly $\alpha$ ) absorbers depends on the ionizing background and IGM gas density. In photoionization equilibrium, the density of neutral hydrogen in low-density gas is given by

$$n_{\text{HI}} = \frac{n_e n_H \alpha_H^{(A)}}{\Gamma_H}, \quad (4)$$

where  $n_e = (1 + 2y) = 1.165n_H$  is the electron density for fully ionized gas,  $n_H$  is the total density of hydrogen nuclei, and  $y = n_{\text{He}}/n_{\text{H}} = [(Y/4)/(1 - Y)] \approx 0.0823$  is the helium-

to-hydrogen ratio by number, assuming  $Y = 0.2477$  helium abundance by mass. For the low values of  $n_H$  and  $N_{\text{HI}}$  in these IGM absorbers, we adopt the hydrogen case-A radiative recombination rate coefficient,  $\alpha_H^{(A)}(T) \approx (2.51 \times 10^{-13} \text{ cm}^3 \text{ s}^{-1}) T_{4.3}^{-0.726}$ , scaled to an electron temperature  $T = (10^{4.3} \text{ K}) T_{4.3}$  characteristic of low-metallicity IGM (Donahue & Shull 1991). The H I photoionization rate depends on the metagalactic radiation field, with specific intensity  $I_\nu = I_0(\nu/\nu_0)^{-\alpha_s}$  referenced to the Lyman limit,  $h\nu_0 = 13.6 \text{ eV}$ . Here,  $\langle \alpha_s \rangle \approx 1.8$  is the mean QSO spectral index between 1.0–1.5 ryd (Telfer et al. 2002). The frequency-integrated photoionization rate is given by the approximate formula,

$$\Gamma_H \approx \frac{4\pi I_0 \sigma_0}{h(\alpha_s + 3)} \approx (2.49 \times 10^{-14} \text{ s}^{-1}) I_{-23} \left( \frac{4.8}{\alpha_s + 3} \right), \quad (5)$$

where we adopt  $I_0 = (10^{-23} \text{ erg cm}^{-2} \text{ s}^{-1} \text{ Hz}^{-1} \text{ sr}^{-1}) I_{-23}$ . Hereafter, we combine the two parameters,  $I_0$  and  $\alpha_s$ , into a single scaling parameter,  $\Gamma_{-14} = (\Gamma_H/10^{-14} \text{ s}^{-1})$ , for the hydrogen photoionization rate. Previous calculations of the low- $z$  ionizing intensity (Shull et al. 1999) found  $\Gamma_H \approx 3.2_{-1.2}^{+2.0} \times 10^{-14} \text{ s}^{-1}$  and noted that low- $z$  observational constraints were consistent with values in this range. More recent calculations (Haardt & Madau 2011) are consistent with Equation (5) and other estimates at  $z \approx 0$ . The rising hydrogen ionizing rate can be fitted by  $\Gamma_H = (2.28 \times 10^{-14} \text{ s}^{-1})(1+z)^{4.4}$ , consistent with estimates at  $z \approx 0$ . Figure 7 illustrates current estimates of the intensity of the metagalactic ionizing radiation field starting at 1 ryd (H I photoionization edge), continuing to 4 ryd (He II edge) and beyond, including ionization potentials needed to produce some of the higher metal ions, such as C IV (47.87 eV = 3.52 ryd), O VI (113.87 eV = 8.37 ryd), O VII (138.08 eV = 10.15 ryd), Ne VIII (207.2 eV = 15.24 ryd), and O VIII (739.11 eV = 54.35 ryd).

The Ly $\alpha$  absorbers are thought to arise as fluctuations in dark-matter confined clumps or filaments, which we approximate as singular isothermal spheres, with density profiles,  $n_H(r) = n_0(r/r_0)^{-2}$  normalized to a fiducial radius  $r_0$ . For a sight line passing through an absorber at impact parameter  $p$ , the total baryon mass within radius  $r = p$  is  $M_b(p) = 4\pi\mu_b n_0 r_0^2 p$ , where  $\mu_b = (1 + 4y)m_H \approx 1.33m_H$  is the mean baryon mass per hydrogen. The H I column density can be derived, using the density-squared dependence of  $n_{\text{HI}}$  and integrating through the cloud along pathlength  $\ell$  at impact parameter  $p$ , where  $\ell^2 = r^2 - p^2$ . We substitute  $p = r \cos \phi$  and  $\ell = p \tan \phi$  for the angle  $\phi$  between the directions of  $p$  and  $r$ ,

$$N_{\text{HI}}(p) = \left[ \frac{\alpha_H^{(A)}(1+2y)}{\Gamma_H} \right] 2 \int_0^\infty n_0^2 \left( \frac{r}{r_0} \right)^{-4} dl = \left[ \frac{\pi n_0^2 r_0^4 \alpha_H^{(A)}(1+2y)}{2\Gamma_H p^3} \right]. \quad (6)$$

Solving for the quantity  $n_0 r_0^2$ , we can express the absorber mass within  $r = p$  as

$$M_b(p) = 4\pi\mu_b p^{5/2} \left[ \frac{2\Gamma_H N_{\text{HI}}(p)}{\pi(1+2y)\alpha_H^{(A)}} \right]^{1/2} = (1.09 \times 10^9 M_\odot) \left[ N_{14}^{1/2} \Gamma_{-14}^{1/2} p_{100}^{5/2} T_{4.3}^{0.363} \right]. \quad (7)$$

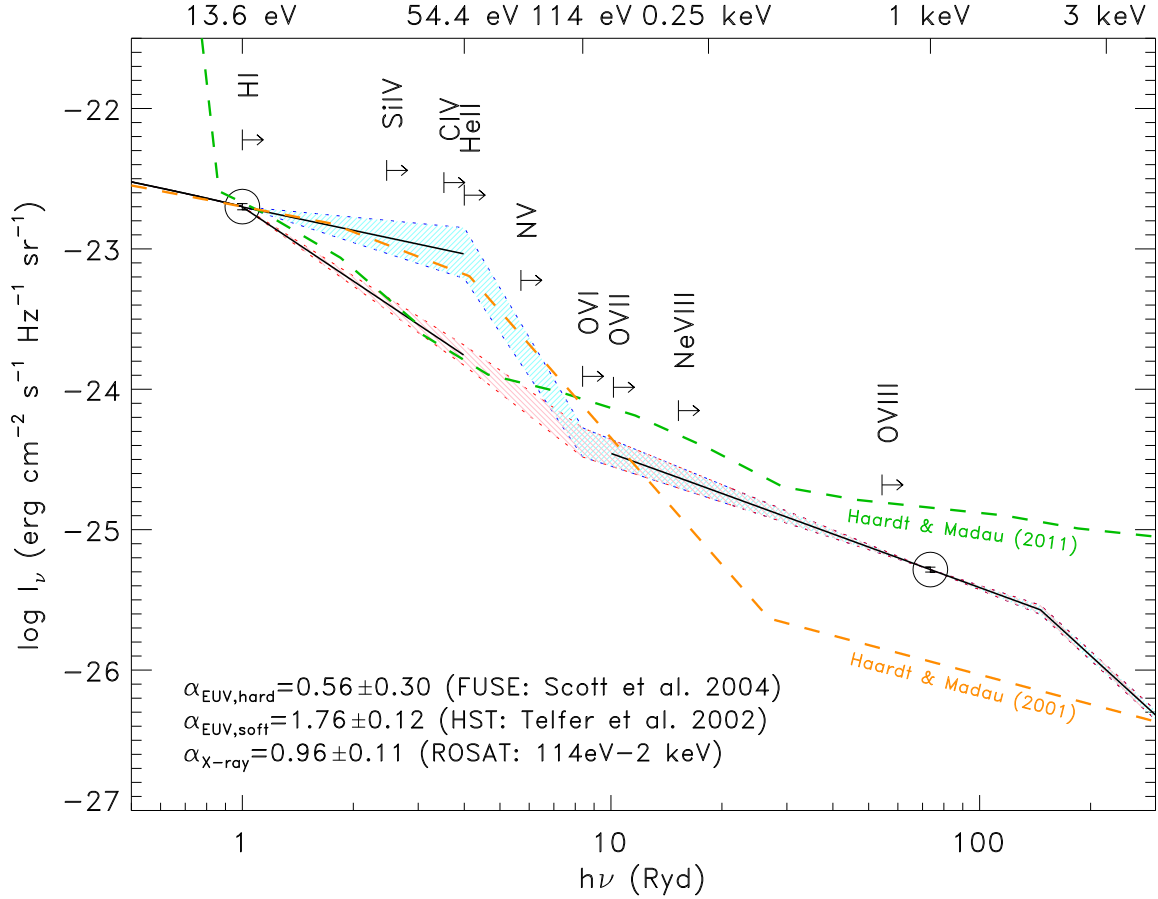


Fig. 7.— Compilation of the mean AGN spectral energy distribution (SED), pinned at 1 ryd, with  $I_0 = 2 \times 10^{-23}$  erg cm $^{-2}$  s $^{-1}$  Hz $^{-1}$  sr $^{-1}$  and two different flux distributions,  $F_\nu \propto \nu^{-\alpha_s}$ . Previous composite spectra from small numbers of AGN are shown in red (HST) and light blue (FUSE), with slopes  $\alpha_s = 1.76 \pm 0.12$  (Telfer et al. 2002) and  $\alpha_s = 0.56^{+0.38}_{-0.28}$  (Scott et al. 2004). Soft X-ray data are from ROSAT observations of AGN in the Lockman Hole (Hasinger 1994) normalized at  $E = 1$  keV (73.53 ryd) with spectral slope  $F_E \propto E^{-0.96 \pm 0.11}$ . The ionization potentials of H I and He II and ionization energies to produce key metal ions are shown as arrows. The metagalactic backgrounds from Haardt & Madau (2001, 2011) are over-plotted.



In the above formula, we have scaled the impact parameter  $p = (100 \text{ kpc})p_{100}$  using a 100-kpc characteristic scale length of Ly $\alpha$  absorbers; see Penton et al. (2000) and references therein. We scale the H I column density to a characteristic value,  $N_{\text{HI}} = (10^{14} \text{ cm}^{-2})N_{14}$ .

Next, we calculate the baryon density in the Ly $\alpha$  absorbers as a fraction of the cosmological closure density,  $\rho_{\text{cr}} = (3H_0^2/8\pi G)$  at  $z = 0$ . Because our Ly $\alpha$  survey extends to  $z = 0.4$ , we include corrections for cosmological evolution in the space density of absorbers,  $\phi(z) \propto (1+z)^3$ , and the rising hydrogen photoionization rate,  $\Gamma_H(z) \propto (1+z)^{4.4}$ . We begin with the standard expression for the number of absorbers per unit redshift,

$$\frac{d\mathcal{N}}{dz} = \left[ \frac{c}{(1+z)H(z)} \right] \pi [p(z)]^2 \phi(z), \quad (8)$$

where  $H(z) = H_0[\Omega_m(1+z)^3 + \Omega_\Lambda]^{1/2}$  is the Hubble parameter at redshift  $z$  in a flat  $\Lambda$ CDM cosmology, and the absorber space density is  $\phi(z) = \phi_0(1+z)^3$ . The absorption-line frequency and impact parameter  $p$  correspond to the H I column density and absorber mass given in Equations (6) and (7). The baryon mass density in Ly $\alpha$  absorbers at redshift  $z$  is written as the product of absorber mass,  $M_b$ , times the absorber space density,  $\phi(z)$ , integrated over the distribution in H I column density. We define the closure parameter,  $\Omega_b^{(\text{HI})} = \rho_b(0)/\rho_{\text{cr}}(0)$  at  $z = 0$ , where  $\rho_b(z) = \rho_b(0)(1+z)^3$ . Assembling all the terms from Equations (6–8), we find a ( $z = 0$ ) closure parameter in Ly $\alpha$  absorbers, of column density  $N_{\text{HI}}$ .

$$\Omega_b^{(\text{HI})} = \frac{\phi_0 M_b}{\rho_{\text{cr}}} = \frac{32(2\pi)^{1/2}}{3} \left[ \frac{\mu_b G}{cH(z)(1+z)^2} \right] \left[ \frac{\Gamma_H(z)p(z)N_{\text{HI}}}{(1+2y)\alpha_H^{(a)}} \right]^{1/2}. \quad (9)$$

From recent calculations of the metagalactic ionizing background (Haardt & Madau 2011), the hydrogen photoionization rate rises rapidly from redshifts  $z = 0$  to  $z = 0.7$ , and can be fitted to the formula  $\Gamma_{-14} = (2.28)(1+z)^{4.4}$ . We have little data on the redshift evolution of the characteristic absorber scale length,  $p$ , other than theoretical expectations for the gravitational instability of filaments in the cosmic web. In the following calculation, we assume that  $p = (100 \text{ kpc})p_{100}$ , remains constant with redshift. With these and other parameterizations, we can re-write Equation (9) as

$$\begin{aligned} \Omega_b^{(\text{HI})} &= (6.0 \times 10^{-5}) \frac{h_{70}^{-1} \Gamma_{-14}^{1/2} p_{100}^{1/2} T_{4.3}^{0.363}}{(1+z)^2 H(z)/H_0} \int_{N_{\text{min}}}^{N_{\text{max}}} \frac{d\mathcal{N}(\log N_{\text{HI}})}{dz} N_{14}^{1/2} d(\log N_{\text{HI}}) \\ &= (9.0 \times 10^{-5}) \frac{h_{70}^{-1} p_{100}^{1/2} T_{4.3}^{0.363} (1+z)^{0.2}}{[\Omega_m(1+z)^3 + \Omega_\Lambda]^{1/2}} \int_{N_{\text{min}}}^{N_{\text{max}}} \frac{d\mathcal{N}(\log N_{\text{HI}})}{dz} N_{14}^{1/2} d(\log N_{\text{HI}}) \quad (10) \end{aligned}$$

The ionization rate,  $\Gamma_{-14} \propto (1+z)^{4.4}$ , entering Equation (10) as the square-root, almost exactly compensates for the  $(1+z)^2$  factor in the denominator. The above formulae describe

the H I photoionization corrections used to convert the column-density distribution of Ly $\alpha$  absorbers into total baryon density.

From UV spectrographic surveys of intergalactic Ly $\alpha$  absorbers, we now have a reasonable understanding of the distribution of H I column densities in the diffuse Ly $\alpha$  forest (Penton et al. 2000, 2004; Danforth & Shull 2008; Lehner et al. 2007). Penton et al. (2004) applied photoionization corrections to a survey of 187 Ly $\alpha$  absorbers over redshift path-length  $\Delta z = 1.157$ . They found that Ly $\alpha$  absorbers have a distribution in H I column density  $f(N) \propto N^{-\beta}$  with  $\beta = 1.65 \pm 0.07$  and contribute  $29 \pm 4\%$  to the total baryon content. Danforth & Shull (2008) surveyed 650 Ly $\alpha$  absorbers with *HST*/STIS over the range  $12.5 \leq \log N_{\text{HI}} \leq 16.5$  with total pathlength  $\Delta z = 5.27$ . Their H I distribution was similar, with  $\beta = 1.73 \pm 0.04$  and a fractional contribution of  $28.7 \pm 3.7\%$  (statistical errors only) to the baryon census<sup>2</sup>. In a reanalysis of the Ly $\alpha$  data from *HST* and *FUSE*, our group (Tilton et al. 2012, in preparation) studied 723 Ly $\alpha$  systems with column densities between  $12.5 < \log N_{\text{HI}} < 16.5$ . The new derivation of  $\Omega_b^{(\text{HI})}$  is consistent with 25-30% of the baryons residing in the Ly $\alpha$  forest and partial Lyman-limit systems. For the current census, we adopt a baryon fraction of  $\Omega_b^{(\text{HI})} = 28 \pm 11\%$ . The latter error bars include systematic effects,

We now summarize the current status of the error budgets for the major contributors to uncertainty in the diffuse Ly $\alpha$  forest baryon census. Many of the scalings enter the formula for  $\Omega_b^{(\text{HI})}$  as the square root, a weak dependence arising because recombination theory predicts that  $N_{\text{HI}} \propto n_H^2$  for highly ionized absorbers. Thus, the total baryon mass (proportional to  $n_H$ ) depends on a weight factor,  $N_{14}^{1/2}$  (see equations [7] and [9]). From this formulation, we can conduct an error-propagation analysis, to arrive at the overall uncertainty on the Ly $\alpha$  contribution to  $\Omega_b$  in eq. (10). This quantity depends on five parameters, which we list below with assigned errors.

1. **Distribution of H I column densities.** Danforth & Shull (2008) measured the distribution of H I column densities,  $d\mathcal{N}/dz \propto N_{\text{HI}}^{-\beta}$ . Based on 650 low-redshift Ly $\alpha$  absorbers, they found a slope  $\beta \approx 1.73 \pm 0.04$  and a baryon content of  $29 \pm 4\%$  of  $\Omega_b$ , integrated over  $12.5 \leq \log N_{\text{HI}} \leq 16.5$ . Our newer survey (Tilton et al. 2012) finds that the Ly $\alpha$ -forest plus partial Lyman-limit systems contribute  $\sim 28 \pm 4\%$  to the baryon fraction. We assume 15% uncertainty in the column-density distribution statistics, which are increasingly uncertain at  $\log N_{\text{HI}} < 13.0$ . Extending the  $N_{\text{HI}}^{-1.73}$  distribution

---

<sup>2</sup>Although the formulae for baryon fractions were stated correctly (Equations 7–10 in Danforth & Shull 2008), the values listed in their Tables 12 and 13 over-estimated values of  $\Omega_b$  from H I and O VI. Our new survey (Tilton et al. 2012) discusses these effects, properly includes effects of redshift evolution as noted above, and updates the H I-traced baryon fraction.

from  $\log N = 12.5$  to  $12.0$  would add another 3% to the baryon fraction (from 28% to 31%) if there is no change in slope.

2. **Hydrogen photoionization rate.** This rate,  $\Gamma_H$ , depends on the radiation field normalization at 1 ryd ( $I_0$ ) and spectral slope ( $\alpha_s$ ) between 1.0–1.5 ryd, neither of which is well determined at present (Telfer et al. 2002; Scott et al. 2004). Our calculation takes into account the  $(1+z)^{4.4}$  rise in  $\Gamma_H(z)$  from  $z = 0$  to  $z = 0.7$ , a fit to the recent calculations of Haardt & Madau (2011). We estimate the joint error on  $\Gamma_H$  as  $\pm 50\%$ , from models of the metagalactic radiation field from quasars and galaxies (Shull et al. 1999; Haardt & Madau 2011).
3. **Characteristic scale-length of absorbers.** The characteristic impact parameter,  $p_{100}$ , in units of 100 kpc is inferred by direct and indirect means, including comparing “hits and misses” of Ly $\alpha$  absorbers along nearby sight lines and the cumulative distributions of absorbers with nearest-neighbor galaxies (Stocke et al. 1995; Shull et al. 1998). The frequency of Ly $\alpha$  absorption lines per unit redshift also implies 200–300 kpc absorber cross sections, when associated with the space density of galaxies down to luminosities  $L \approx 0.01 - 0.03L^*$  (Shull et al. 1996; Stocke et al. 2006; Prochaska et al. 2011). We adopt an uncertainty of  $\pm 50\%$  on  $p_{100}$ .
4. **Electron temperature.** Temperature ( $T_e$ ) enters through the square root of the hydrogen recombination rate coefficient,  $\alpha_H^{(A)} \propto T^{-0.726}$ . Models of IGM photoelectric heating (Donahue & Shull 1991) predict a range from 5000 K to 30,000 K. For  $z < 0.4$ , with small expected variations from photoionization, we adopt an uncertainty of  $\pm 30\%$ .
5. **Hubble constant.** This parameter has been measured as  $H_0 = 72 \pm 8 \text{ km s}^{-1} \text{ Mpc}^{-1}$  (Freedman et al. 2001) and  $H_0 = 73.8 \pm 2.4 \text{ km s}^{-1} \text{ Mpc}^{-1}$  (Riess et al. 2011), using distance scales based on Cepheids in galaxies with Type Ia supernovae. To be conservative, we adopt an error of  $\pm 5\%$ .

From standard error-propagation formulae, we write the relative error on  $\Omega_b^{(\text{HI})}$  as the quadrature sum of relative errors on the five parameters, weighted by the square of the exponents (1, 0.5, or 0.363) as they appear in the scaling (see equations 9 and 10):

$$\left(\frac{\sigma_\Omega}{\Omega}\right)^2 = \left(\frac{\sigma_N}{N}\right)^2 + \left(\frac{\sigma_h}{h}\right)^2 + \left(\frac{\sigma_N}{N}\right)^2 + (0.5)^2 \left[ \left(\frac{\sigma_\Gamma}{\Gamma}\right)^2 + \left(\frac{\sigma_p}{p}\right)^2 \right] + (0.363)^2 \left(\frac{\sigma_T}{T}\right)^2 \quad (11)$$

This formula gives a relative error  $(\sigma_\Omega/\Omega) = 0.40$ , so that we can express  $\Omega_b^{(\text{HI})}/\Omega_b^{(\text{tot})} = 0.28 \pm 0.11$ . Most (77%) of the error budget comes from uncertainties in the ionizing radiation field ( $\Gamma_H$ ) and characteristic absorber size ( $p_{100}$ ).

#### 4. SUMMARY OF BARYON CENSUS

Figure 8 shows a pie chart of the current observable distribution of low-redshift baryons in various forms, from collapsed structures to various phases of the IGM and WHIM. These slices show the individual contributions,  $\Omega_b^{(i)}/\Omega_b^{(\text{tot})}$ , to the total baryon content from phase components (*i*). We also discuss previous estimates and uncertainties.

- **Photoionized Ly $\alpha$  Absorbers.** For this paper, we adopt  $\Omega_b^{(\text{HI})} = 28 \pm 11\%$  based on the results of Danforth & Shull (2008), our new survey (Tilton et al. 2012), and the systematic uncertainties discussed in Section 3.2. The mid-range distribution in column densities,  $13.0 < \log N_{\text{HI}} < 14.5$ , is fairly well characterized, but the numbers of high-column absorbers are small. Their contribution to  $\Omega_b$  remains uncertain owing to corrections for their size and neutral fraction. At the low end of the column-density distribution, there could be modest contributions to the baryon content from weaker Ly $\alpha$  absorbers. In current surveys, their numbers are increasingly uncertain at  $\log N_{\text{HI}} < 13$  (our integration was down to 12.5). For a power-law distribution with  $\beta = 1.73$ , extending the distribution from  $\log N = 12.5$  down to 12.0 would increase the baryon fraction by another 10% (from 28% to 31%). For this paper, we adopt  $\Omega_b^{(\text{HI})} = 28 \pm 11\%$  based on the results of Danforth & Shull (2008), Tilton et al. (2012), and the systematic uncertainties discussed in Section 3.2.
- **WHIM (O VI-traced).** Previous *FUSE* surveys of intergalactic O VI absorbers (Danforth & Shull 2005; Tripp et al. 2006) found lower limits of  $\sim 5\%$  and  $7\%$ , respectively for the contribution of this gas to the baryon inventory. These surveys assumed oxygen metallicity  $Z_{\text{O}} = 0.1Z_{\odot}$  and ionization fraction  $f_{\text{OVI}} = 0.2$ . In 2008, three O VI surveys with *HST*/STIS (Danforth & Shull 2008; Tripp et al. 2008; Thom & Chen 2008) probed to lower O VI column densities. Based on the survey of 83 O VI absorbers, Danforth & Shull (2008) and our more recent analysis of 111 O VI absorbers (Tilton et al. 2012), we adopt a baryon fraction  $\Omega_b^{(\text{OVI})} = 15 \pm 4\%$ . The nearly factor-of-two increase arises primarily from our revised corrections,  $(Z_{\text{O}}/Z_{\odot}) f_{\text{OVI}} = 0.01$ , for metallicity and O VI ionization fraction (see Section 3.1).
- **WHIM (BLA-traced).** Broad Ly $\alpha$  absorbers (BLAs) were proposed (Richter et al. 2004, 2006; Lehner et al. 2006, 2007) as repositories of a substantial fraction of the low-redshift baryons. BLAs are defined as Ly $\alpha$  absorbers with Doppler parameters  $b \geq 40 \text{ km s}^{-1}$ , corresponding to temperatures  $T = (m_{\text{H}}b^2/2k) = (9.69 \times 10^4 \text{ K})b_{40}^2$  for pure thermal broadening with  $b = (40 \text{ km s}^{-1})b_{40}$ . Owing to the large abundance of hydrogen, a small neutral fraction (H I) remains detectable in Ly $\alpha$  up to temperatures  $\sim 10^6 \text{ K}$ , although high-S/N is required to measure the broad, shallow absorption. As

a result, the surveys of BLAs differ considerably. In their survey of seven AGN sight lines, Lehner et al. (2007) found a BLA frequency of  $d\mathcal{N}/dz = 30 \pm 4$  for absorbers with  $40 \leq b \leq 150 \text{ km s}^{-1}$  and  $\log N_{\text{HI}} \geq 13.2$ . They claimed that 20% of the baryons reside in BLAs. A more recent survey (Danforth et al. 2010) came to different conclusions. Surveying BLA candidates along seven AGN sight lines observed by HST/STIS, their BLA absorption-line frequency per unit redshift was  $d\mathcal{N}/dz = 18 \pm 11$ , comparable to that of the O VI absorbers but 40% lower than that found by Lehnert et al. (2007). After accounting for possible (20–40%) overlap between BLA and O VI (metal-bearing) absorbers, the corresponding baryon fraction is  $\Omega_{\text{BLA}}/\Omega_b = 0.14^{+0.024}_{-0.018}$ . For Figure 8, we adopt a value of  $15 \pm 7\%$ , with an increased error reflecting the uncertain detection statistics. We apply their metallicity-based correction to obtain a blended total (approximately 1/4 overlap) of  $25 \pm 8\%$  for the O VI/BLA-traced WHIM over the temperature range  $5 \leq \log T \leq 6$ .

- **Galaxies.** Salucci & Persic (1999) found that galaxies contribute 7% of the baryons. More recent discussion by Fukugita & Peebles (2004) estimated 6%. In Figure 8, we assume that galaxies contribute  $7 \pm 2\%$  of the baryons.
- **Groups and Clusters.** The integrated cluster mass function of Bahcall & Cen (1993) was used by Fukugita et al. (1998) to find that the baryon contribution of clusters of galaxies consists of  $\Omega_b^{(\text{stars})} = 0.00155h^{-1.5}$  and  $\Omega_b^{(\text{gas})} = 0.003h^{-1}$ . Adjusting for  $h = 0.7$ , we find a cluster contribution of  $\Omega_b^{(\text{cl})} = 0.00308$  or 6.8% of the baryons. Fukugita & Peebles (2004) revised the hot-baryon contribution to  $\Omega_b^{(\text{cl})} = 0.0018 \pm 0.0007$  or 4% of the baryons, owing to a redefinition of cluster mass (Reiprich & Böhringer 2002). For the total contribution of galaxy clusters, including their hot gas, we adopt a fraction  $4.0 \pm 1.5\%$  of the baryons.
- **Cold H I (and He I) Gas.** Zwaan et al. (2003) and Rosenberg & Schneider (2003) conducted blind H I surveys in the 21-cm line that probe the mass density in neutral atomic gas. The HIPASS survey (Zwaan et al. 2003) found  $\Omega_{\text{HI}} = (4.7 \pm 0.7) \times 10^{-4}$ . Following the discussion of Fukugita & Peebles (2004), which augments the H I measurements by the expected accompanying cold He I and H<sub>2</sub>, we plot the total cold gas mass in Figure 8 as  $1.7 \pm 0.4\%$  of the baryons.
- **Circumgalactic Medium (CGM).** X-ray spectra of AGN taken with both *Chandra* and *XMM/Newton* detect O VII absorbers at  $z \approx 0$  (see Bregman 2007; McKernan et al. 2005; Wang et al. 2005; Fang et al. 2006). The typical detected column densities,  $N_{\text{OVII}} \approx 10^{16} \text{ cm}^{-2}$ , correspond to ionized hydrogen column densities  $N_{\text{HII}} \approx 10^{20} \text{ cm}^{-2}$  assuming a length-scale  $\sim 10 \text{ kpc}$  and mean metallicity of 20% solar. Several arguments suggest that the Galactic O VII resides in a thick disk or low scale-length

halo (5–10 kpc; see Yao & Wang 2005). Such a reservoir holds  $\sim 10^9 M_\odot$  which is  $\sim 2\%$  of the  $5 \times 10^{11} M_\odot$  in Milky Way baryons. Bregman (2007) suggested that a hot gaseous medium with mass  $\sim 10^{10} M_\odot$  might extend throughout the Local Group. This reservoir is also  $\sim 2\%$  of the  $6 \times 10^{11} M_\odot$  baryonic mass of the Local Group, assuming total mass  $5 \times 10^{12} M_\odot$  and 12% baryon fraction (McGaugh et al. 2010). However, the Milky Way halo and Local Group may not be typical of star-forming galaxies. Additional CGM could extend to distances of 100–200 kpc from galaxies with higher specific star formation rates (Stocke et al. 2006). Savage et al. (2010) detected hot circumgalactic gas ( $\log T = 5.8 - 6.2$ ) in H I-free O VI absorption associated with a pair (and perhaps small group) of galaxies at  $z \approx 0.167$ , at impact parameters  $p \approx 100$  kpc. These authors note that the absence of H I absorption with broad O VI suggests a “rare but important class of low- $z$  intergalactic medium absorbers”.

Prochaska et al. (2011) took this idea further, suggesting that *all* the O VI arises in the “extended CGM of sub- $L^*$  galaxies”. Their mass estimate associates the O VI absorption with galaxies ( $0.1 < L/L^* < L^*$ ) having constant hydrogen column densities,  $N_H = 10^{19} \text{ cm}^{-2}$ , over the full 200–300 kpc extent, as gauged by AGN-galaxy impact parameters. They estimated that these extended halos could contain a mass  $M_{\text{CGM}} \approx (3 \times 10^{10} M_\odot)(r_{\text{CGM}}/300 \text{ kpc})^2$ , which would represent  $\sim 50\%$  of the baryon masses of present-day sub- $L^*$  galaxies. They further assert that gas at these large distances is gravitationally bound and virialized. We question the realism of constant- $N$ , virialized gas at such large distances from dwarf galaxies. Previous nearest-neighbor studies low- $z$  O VI absorbers and galaxies (Stocke et al. 2006; Wakker & Savage 2009) found correlations with  $L^*$  galaxies (at 800 kpc) and with dwarf ( $0.1L^*$ ) galaxies (at 200 kpc). For Figure 8, we adopt a CGM contribution of  $5 \pm 3\%$ , recognizing that the CGM reservoir is still poorly understood.

We now summarize the current state of the low- $z$  baryon census and discuss future issues. As shown in Figure 8, observational measurements of Ly $\alpha$ , O VI, and broad Ly $\alpha$  absorbers, together with more careful corrections for metallicity and ionization fraction, can account for  $\sim 60\%$  of the baryons in the intergalactic medium. An additional 10% may reside in circumgalactic gas and 10% in galaxies and clusters. This still leaves a substantial fraction,  $25 \pm 15\%$ , unaccounted for. We have tried to assign realistic errors on each of the “slices of the baryon pie”, most of which involve systematic uncertainties in the parameters need for the ionization corrections, metallicity, and geometric factors (cloud size). Thus, it is possible that the baryon inventory could change, as a result of better determinations of these parameters. However, most numerical simulations, including ours, suggest that a substantial reservoir of hot baryons exists in the hotter WHIM ( $T > 10^6$  K).

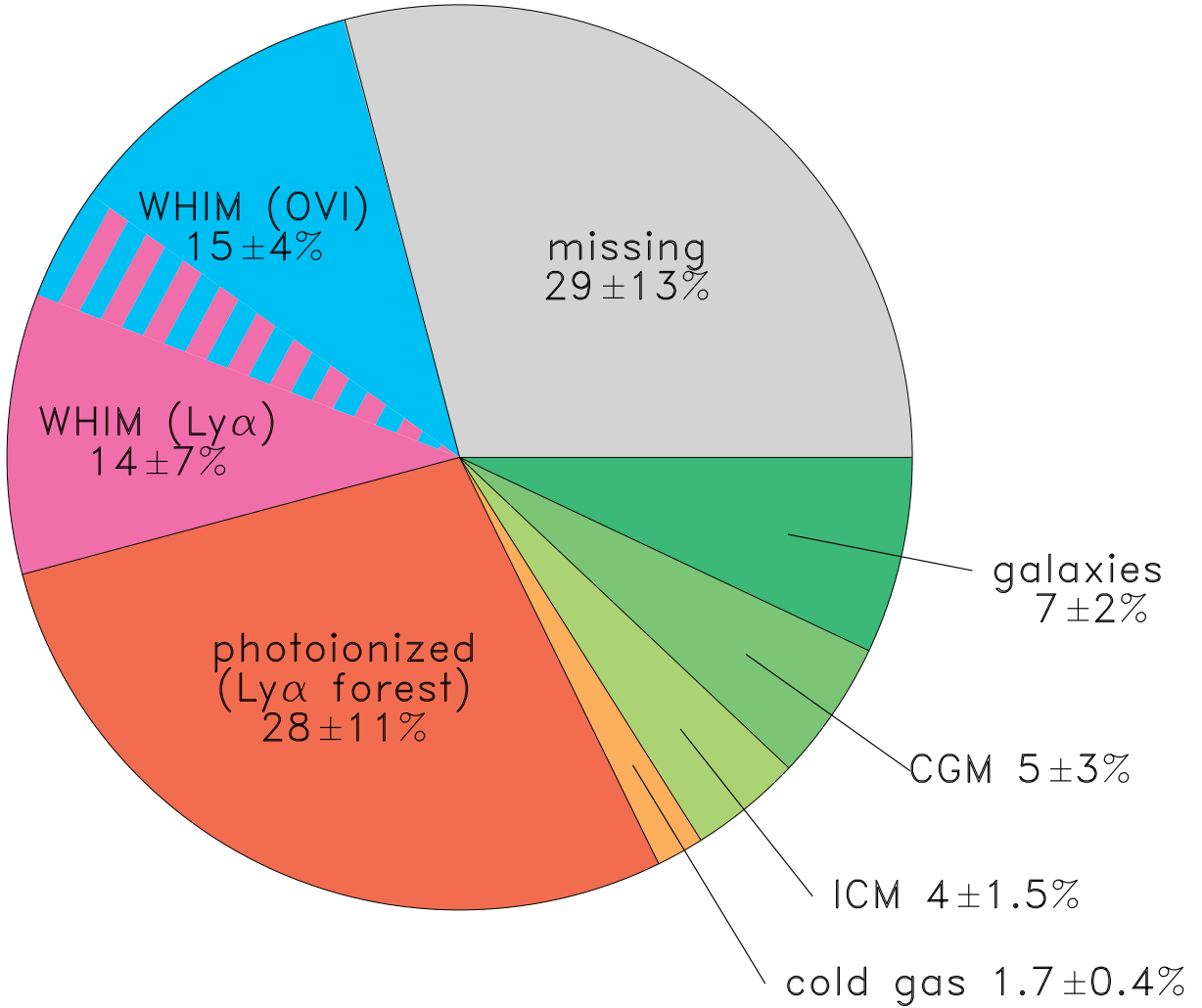


Fig. 8.— Compilation of the current observational measurements of the low-redshift baryon census (Section 3.3). Slices of the pie-chart show baryons in collapsed form (galaxies, groups, clusters), in the circumgalactic medium (CGM) and intercluster medium (ICM), and in cold gas (H I and He I). Large reservoirs include diffuse photoionized  $\text{Ly}\alpha$  forest, and WHIM traced by O VI and broad  $\text{Ly}\alpha$  absorbers. Blended colors (BLAs and O VI) have combined total of  $25 \pm 8\%$ , accounting for double-counting of WHIM at  $10^5 - 10^6$  K with detectable metal ions. The collapsed phases (galaxies, CGM, ICM, cold neutral gas) total  $18 \pm 4\%$ . Formally,  $29 \pm 13\%$  of the baryons remain unaccounted for. Some could be detected in hotter, X-ray absorbing WHIM at  $T \geq 10^6$  K. Large error bars on other IGM phases allow additional “missing baryons” in photoionized gas and low-column density O VI and  $\text{Ly}\alpha$  absorbers. Deeper spectroscopic UV and X-ray surveys are needed to resolve this issue.

What observations and theoretical work are needed to make progress, either on error bars or in baryon detections? First, we need more precise UV absorption-line surveys to measure O VI and Ly $\alpha$  absorbers to lower column densities. As described in Section 3, the numbers in current surveys become increasingly uncertain at column densities  $\log N_{\text{HI}} < 13.0$  and  $\log N_{\text{OVI}} < 13.5$ . The current surveys integrate below these levels, but our experience using COS to re-examine earlier Ly $\alpha$  and O VI detections with FUSE, GHRS, and STIS, suggests that some of these weak absorbers are not confirmed with high-S/N data. As part of an *HST* Archive Legacy Project, we are reanalyzing O VI and Ly $\alpha$  data from *HST*/STIS (Tilton, Danforth, & Shull 2012) to provide critically evaluated column densities for  $N_{\text{HI}}$  and  $N_{\text{OVI}}$ , and their absorption-line frequencies,  $d\mathcal{N}/dz$ . The O VI data will be integrated with our fits to  $f_{\text{OVI}} Z_{\text{O}}$  to yield more accurate values of  $\Omega_b^{(\text{OVI})}$ .

However, we can do even better with the 10-fold increase in UV sensitivity throughput of Cosmic Origins Spectrograph on *HST*. We recommend that *HST*/COS be used to obtain high-quality data ( $S/N \geq 30$ ) to search for additional baryons in weak absorbers, and to constrain the predicted flattening in the column density distributions of H I and O VI. Scaled to column densities  $(10^{13} \text{ cm}^{-2})N_{13}$ , these lines have equivalent widths of  $(12.5 \text{ m}\text{\AA})N_{13}$  (for O VI  $\lambda 1032$ ) and  $(54.5 \text{ m}\text{\AA})N_{13}$  (for Ly $\alpha$ ). These weak-absorber surveys require *HST*/COS sensitivity to 4 m $\text{\AA}$  absorbers, which is achievable at  $S/N = 30$  toward many bright AGN background targets. Our simulations suggest that increasing numbers of H I and O VI absorbers exist at these levels, with some flattening at  $\log N_{\text{OVI}} \leq 12.0$  (see Fig. 2).

We can also use COS to obtain better detections and statistics for broad Ly $\alpha$  absorbers (BLAs) and the Ne VIII doublet ( $\lambda\lambda 770.4, 780.3$ ). The Ne VIII lines are potentially more reliable probes of hot, collisionally ionized gas than O VI, since Ne VIII requires 207 eV to produce and is likely to be less contaminated by photoionization. The lower solar neon abundance,  $(\text{Ne}/\text{O})_{\odot} \approx 0.15$ , makes the Ne VIII lines weak, and redshifts  $z > 0.47$  are needed to shift them into the *HST*/COS band. The BLAs have considerable promise for WHIM probes, as they do not require corrections for metallicity. They do require a determination of the neutral fraction,  $f_{\text{HI}}$ , which involves careful modeling of the gas temperature and ionization conditions (e.g., Danforth, Stocke, & Shull 2010).

This effect is clearly the case with the claimed X-ray detections of O VII in the WHIM (Nicastro et al. 2005) which are not confirmed in other data (e.g., Kaastra et al. 2006; Rasmussen et al. 2007) or in re-analysis of the same data (Yao et al. 2011). Therefore, the most critical observations for WHIM census may require a next generation of X-ray spectrographs, to measure the weak absorption lines of O VII  $\lambda 21.602$ , O VIII  $\lambda 18.969$ , and other He-like and H-like lines of abundant metals (C V, C VI, N VI, N VII). As discussed by Yao et al. (2012), this requires high-throughput spectrographs ( $E \approx 0.2 - 1.0 \text{ keV}$ ) with energy resolution



$E/\Delta E > 4000$  sufficient to resolve O VII (21.602 Å) absorbers with mÅ equivalent width. For weak lines, the predicted equivalent widths are  $W_\lambda = (2.88 \text{ mÅ})(N_{\text{OVII}}/10^{15} \text{ cm}^{-2})$ .

Finally, the IGM simulations need to be improved in several aspects, if they are to be used as reliable predictors of crucial IGM parameters (density, temperature, metallicity, and ionization fractions). In this paper, we computed individual (cell-by-cell) values of metallicity  $Z_{\text{O}}$  and ionization fraction  $f_{\text{OVI}}$ , together with their statistical variations and co-variance. Our simulations (Smith et al. 2011) were performed with somewhat larger box sizes ( $50h^{-1}$  Mpc) and on a larger  $1024^3$  grid, compared with previous studies of low- $z$  IGM thermodynamics.

This allowed us to provide more accurate corrections for the product,  $(Z_{\text{O}})/Z_{\odot}f_{\text{OVI}}$ , as a function of column density,  $N_{\text{OVI}}$ . These statistics can be performed for other key ions (O VII, Ne VIII). We will be improving our simulations through higher resolution, the addition of discrete ionizing sources, and radiative transfer. We also will explore the the correct mixture of collisional ionization and photoionization in the WHIM, a project that will require understanding the implications of different feedback mechanisms of injecting mass, thermal energy, and metals into the circumgalactic medium. How these metals mix and radiate are likely to determine the thermodynamics of the surrounding IGM. Because there still exist considerable differences between how simulations treat the thermal state of the IGM, we will continue to push to higher resolution so we can capture the low-mass galaxies which are probably important for metal production and injection into the IGM.

This work was supported by NASA grant NNX08AC14G for COS data analysis and an STScI archival legacy grant AR-11773.01-A. Our theoretical work and numerical simulations were supported by the Astrophysical Theory Program (NNX07-AG77G from NASA and AST07-07474 from NSF) at the University of Colorado Boulder. We thank Eric Hallman, Michele Trenti, John Stocke and Evan Tilton for comments on the manuscript, and Mark Voit for discussions on hot gas in clusters and galaxy halos.

## REFERENCES

- Asplund, M., Grevesse, N., Sauval, A. J., & Scott, P. 2009, *ARA&A*, 47, 481
- Bahcall, N. A., & Cen, R. 1993, *ApJ*, 407, L49
- Bechtold, J., Crotts, A. P. S., Duncan, R. C., & Fang, Y. 1994, *ApJ*, 437, L83
- Bregman, J. N. 2007, *ARA&A*, 45, 221
- Bristow, P. D., & Phillipps, S. 1994, *MNRAS*, 267, 13
- Buote, D., Zappacosta, L., Fang, T., et al. 2009, *ApJ*, 695, 1351
- Bryan, G. & Norman, M. L. 1997, in *Workshop on Structured Adaptive Mesh Refinement Grid Methods*, ed. N. Chrisochoides, IMA Vol. Math., 117, (Springer-Verlag)
- Cen, R., & Chisari, N. E. 2011, *ApJ*, 731, 11
- Cen, R., & Ostriker, J. P. 1999, *ApJ*, 519, L109
- Cen, R., & Ostriker, J. P. 2006, *ApJ*, 650, 560
- Danforth, C. W., Stocke, J. T., & Shull, J. M. 2010, *ApJ*, 710, 613
- Danforth, C. W. 2009, *AIP Conf. Proc.*, Vol. 1135, ed. G. Sonneborn, M. E. van Steenberg, H. W. Moos, & W. P. Blair, 8
- Danforth, C. W., & Shull, J. M. 2008, *ApJ*, 679, 194
- Danforth, C. W., Stocke, J. T., Keeney, B. A., et al. 2011, *ApJ*, 743:18
- Donahue, M., & Shull, J. M. 1991, *ApJ*, 383, 511
- Davé, R., Hernquist, L., Katz, N., & Weinberg, D. H. 1999, *ApJ*, 511, 521
- Davé, R., Cen, R., Ostriker, J.P., et al. 2001, *ApJ*, 552, 473
- Fang, T., Marshall, H. L., Lee, J. C., David, D. S., & Canizares, C. R. 2002, *ApJ*, 572, L127
- Fang, T., McKee, C. F., Canizares, C. R., & Wolfire, M. 2006, *ApJ*, 644, 174
- Fang, T., Canizares, C., & Yao, Y. 2007, *ApJ*, 670, 992
- Fang, T., Buote, D. A., Humphrey, P. J., et al. 2010, *ApJ*, 714, 1715
- Freedman, W. L., Madore, B. F., Gibson, B. K., et al. 2001, *ApJ*, 553, 47
- Fukugita, M., Hogan, C. J., & Peebles, P. J. E. 1998, *ApJ*, 503, 518
- Fukugita, M., & Peebles, P. J. E. 2004, *ApJ*, 616, 643
- Haardt, F., & Madau, P. 2001, in *Clusters of Galaxies and the High Redshift Universe Observed in X-rays*, ed. D. M. Neumann & J. T. V. Tran
- Haardt, F., & Madau, P. 2011, *ApJ*, submitted (arXiv:1105.2039)

- Hasinger, G. 1994, in *Frontiers of Space and Ground-Based Astronomy: The Astrophysics of the 21<sup>st</sup> Century*, ed. W. Wamsteker, M. Longair, Y. Kondo, ASSL, 187, 381
- Kaastra, J., Werner, N., den Herder, J. W., et al. 2006, *ApJ*, 652, 189
- Komatsu, E., Smith, K. M., Dunkley, J., et al. 2011, *ApJS*, 192:18
- Lehner, N., Savage, B., Wakker, B., Sembach, K., & Tripp, T. 2006, *ApJS*, 164, 1
- Lehner, N., Savage, B. D., Richter, P., et al. 2007, *ApJ*, 658, 680
- McGaugh, S. S., Schombert, J. M., de Blok, W. J. G., & Zagursky, M. J. 2010, *ApJ*, 708, L14
- McKernan, B., Yaqoob, T., & Reynolds, C. S. 2005, *MNRAS*, 617, 232
- Narayanan, A., Savage, B. D., & Wakker, B. P., et al. 2009, *ApJ*, 703, 74
- Narayanan, A., Savage, B. D., Wakker, B. P., et al. 2011, *ApJ*, 730:15
- Nicastro, F., Mathur, S., Elvis, M., et al. 2005a, *Nature*, 433, 495
- Nicastro, F., Mathur, S., Elvis, M., et al. 2005b, *ApJ*, 629, 700
- Nicastro, F., Mathur, S., & Elvis, M. 2008, *Science*, 319, 55
- Oppenheimer, B. D., & Davé 2009, *MNRAS*, 395, 1875
- Oppenheimer, B. D., Davé, R., Katz, N., Kollmeier, J. A., & Weinberg, D. H. 2011, *MNRAS*, submitted (arXiv:1106.1444)
- O’Shea, B., Bryan, G., Bordner, J., et al. 2004, in *Adaptive Mesh Refinement*, Springer, astro-ph/0403044, *Introducing Enzo, an AMR Cosmology Application*
- Peimbert, M., Luridiana, V., & Peimbert, A. 2007, *ApJ*, 666, 636
- Penton, S. V., Shull, J. M., & Stocke, J. T. 2000, *ApJ*, 544, 150
- Penton, S. V., Stocke, J. T., & Shull, J. M. 2004, *ApJS*, 152, 29
- Prochaska, J. X., Weiner, B., Chen, H.-W., Mulchaey, J., & Cooksey, K. 2011, *ApJ*, 740:91
- Rasmussen, A., Kahn, S. M., Paerels, F., et al. 2007, *ApJ*, 656, 129
- Reiprich, T. H., & Böhringer, H. 2002, *ApJ*, 567, 716
- Richter, P., Savage, B. D., Tripp, T. M., & Sembach, K. R. 2004, *ApJS*, 153, 165
- Richter, P., Savage, B. D., Sembach, K. R., & Tripp, T. M. 2006, *A&A*, 445, 827
- Riess, A. G., Macri, L., Casertano, S., et al. 2011, *ApJ*, 730, 119
- Rosenberg, J. L., & Schneider, S. E. 2003, *ApJ*, 585, 256
- Salucci, P., & Persic, M. 1999, *MNRAS*, 309, 923

- Savage, B., Lehner, N., Wakker, B., Sembach, K., & Tripp, T. 2005, *ApJ*, 626, 776
- Savage, B., Narayanan, A., Wakker, B., et al. 2010, *ApJ*, 719, 1526
- Scott, J. E., Kriss, G. A., Brotherton, M., et al. 2004, *ApJ*, 615, 135
- Shull, J. M. 2003, in *ASSL*, Vol. 281, *The IGM/Galaxy Connection: Distribution of Baryons at  $z = 0$* , ed. J. L. Rosenberg & M. E. Putman, 1
- Shull, J. M., & Van Steenberg, M. E. 1982, *ApJS*, 48, 95
- Shull, J. M., Stocke, J. T., & Penton, S. V. 1996, *AJ*, 111, 72
- Shull, J. M., Penton, S. V., Stocke, J. T., et al. 1998, *AJ*, 116, 2094
- Shull, J. M., Roberts, D., Giroux, M. L., Penton, S. V., & Fardal, M. A. 1999, *AJ*, 118, 1450
- Smith, B. D., Hallman, E., Shull, J. M., & O’Shea, B. 2011, *ApJ*, 731:6
- Stocke, J. T., Shull, J. M., Penton, S. V., Donahue, M., & Carilli, C. 1995, *ApJ*, 451, 24
- Stocke, J. T., Penton, S. V., Danforth, C. W., et al. 2006, *ApJ*, 641, 217
- Telfer, R., Zheng, W., Kriss, G. A., & Davidsen, A. F. 2002, *ApJ*, 656, 773
- Tepper-García, T., Richter, P., Schaye, J., et al. 2011, *MNRAS*, 413, 190
- Thom, C., & Chen, H.-W. 2008, *ApJS*, 179, 37
- Tripp, T. M., Bowen, D. V., Sembach, K. R., et al. 2006, in *Astrophysics in the Far Ultraviolet*, ed. G. Sonneborn, H. W. Moos, B.-G. Anderson, *ASP Conf. Ser.* 348, 341
- Tripp, T. M., Sembach, K. R., Bowen, D. V., et al. 2008, *ApJS*, 177, 39
- Turk, M. J., Smith, B. D., Oishi, J. S., et al. 2011, *ApJS*, 192, 9
- Wakker, B. P., & Savage, B. D. 2009, *ApJS*, 182, 378
- Wang, Q.-D., Yao, Y., Tripp, T. M., et al. 2005, *ApJ*, 635, 386
- Williams, R., Mathur, S., Nicastro, F., & Elvis, M. 2006, *ApJ*, 642, L95
- Yao, Y., & Wang, Q.-D. 2005, *ApJ*, 624, 751
- Yao, Y., Shull, J. M., Wang, Q.-D., & Cash, W. 2012, *ApJ*, in press
- Zappacosta, L., Nicastro, F., Maiolino, R., et al. 2010, *ApJ*, 714, 74
- Zwaan, M. A., Staveley-Smith, L., Henning, P. A., et al. 2003, *AJ*, 125, 2842